



# The spatiotemporal evolution of atmospheric boundary layers over a thermally heterogeneous landscape

Mary Rose Mangan<sup>1</sup>, Jordi Vilà-Guerau de Arellano<sup>1</sup>, Bart J.H. van Stratum<sup>1</sup>, Marie Lothon<sup>2</sup>,  
Guylaine Canut-Rocafort<sup>3</sup>, and Oscar K. Hartogensis<sup>1</sup>

<sup>1</sup>Meteorology and Air Quality, Wageningen University & Research, Droevendaalsesteeg 4, 6708 PB, Wageningen, the Netherlands

<sup>2</sup>Laboratoire d'Aérodynamique, Université de Toulouse, CNRS, UPS, 14 avenue Edouard Belin 31400, Toulouse, France

<sup>3</sup>CNRM-Université de Toulouse, Météo-France/CNRS, 42 ave. G. Coriolis, 31057, Toulouse, France

**Correspondence:** Mary Rose Mangan (maryrose.mangan@wur.nl)

**Abstract.** We study the diurnal variability of the atmospheric boundary layer (ABL) across spatial scales (between  $\sim 100$  m and  $\sim 10$  km) of irrigation-driven surface heterogeneity in the semi-arid landscape of 2021 LIAISE experiment. We combine observational analysis with the explicit simulation of the ABL using observationally-driven large-eddy simulation (LES) to better understand the physical mechanisms controlling ABL dynamics in heterogeneous regions. Our choice of spatial scales represent current and future single grid cells of global models, which demonstrates how the sources and strength of sub-grid scale heterogeneity vary with model resolution.

From observations, there is a positive buoyancy flux over the irrigated fields driven primarily by moisture fluxes, whereas over the non-irrigated fields, there is a linearly decreasing buoyancy flux profile with height. The surface heterogeneity is felt most strongly near the surface; however, near 1000 m, there appears to be blending zone of mean scalars indicating that the heterogeneity mixes into a new mean state of the atmosphere. There is an stable internal boundary layer of  $\sim 500$  m over the irrigated area. Taking advantage of the three-dimensionality of the LES results, we perform spectral analyses to find that the ABL height had an integral length scale of  $\sim 800$  m matching that of the imposed surface fluxes. Between irrigated and non-irrigated areas, there is an adjustment of the ABL characteristics 500 m upwind of the boundary. We observe a variable-dependent blending zone between scales in the middle of the ABL, but it is limited by the entrainment zone effectively introducing another source of heterogeneity driven by upper atmosphere conditions.

## 1 Introduction

Surface heterogeneity impacts the development of the atmospheric boundary layer (ABL) in a number of ways depending on the atmospheric stability and the strength, size, and orientation of the surface heterogeneity (Bou-Zeid et al., 2020; Brunzell et al., 2011; Hechtel et al., 1990; Huang and Margulis, 2009; Patton et al., 2005; Shen and Leclerc, 1995; van Heerwaarden et al., 2014). Generally, the process-based impacts of surface heterogeneity can be reduced to two classes of impacts: (1) the formation of an internal boundary layer, and (2) the formation of secondary circulations modulated by the meso- and synoptic scales. In this study, we use a combination of observational data from the Land surface Interactions with the Atmosphere over



the Iberian Semi-arid Environment (LIAISE) field experiment and a large-eddy simulation inspired by the results of the observational study to investigate the impacts of unstructured, realistic surface heterogeneity on the development of the ABL. In the LIAISE domain, locally applied irrigation creates a thermal surface heterogeneity. We hypothesize that based on the scale of heterogeneity, the regional LIAISE boundary layer is a composite of a representative ABL from the wet and dry patches (Mangan et al., 2023a). We are motivated to answer the following general research question:

*What physical processes dominate the spatio-temporal evolution of the ABL in a case with realistic surface heterogeneity?*

30

The vertical impact of the surface heterogeneity is largely a function of local stability. Under near neutral conditions, an internal boundary layer can form at the boundary between two patches (Garratt, 1990). Internal boundary layers (IBL) form when the background wind flows across the boundary. The IBL forms at the boundary of the heterogeneity, and it adjusts downwind as it equilibrates with the surface. Typically, IBLs are identified by two mixed-layers in scalar profiles or by vertical flux divergence near the surface (Mahrt, 2000). Mahrt (2000) makes the distinction of the formation of both mesoscale and microscale IBLs that can be formed in reality depending on the patchiness of the land surface and the length scale of the heterogeneity. However, under low wind and convective conditions, secondary circulations can develop (Avisar and Schmidt, 1998; Liu et al., 2011; Maronga et al., 2013; Ouwersloot et al., 2011; Patton et al., 2005; Raasch and Harbusch, 2001; Shen and Leclerc, 1995; van Heerwaarden and Vilà Guerau de Arellano, 2008). Avisar and Schmidt (1998) and Raasch and Harbusch (2001) have found that background winds between 5 and 7  $\text{ms}^{-1}$  eliminate the impact of secondary circulation, but the effect of the background wind depends on the orientation of the wind with respect to the boundary. In addition to the background wind and stability, secondary circulation also depend on the scale of heterogeneity with respect to the ABL depth and ABL turbulence scales. The ABL is most impacted when the scale of the heterogeneity is on the same order of magnitude as the ABL depth (Patton et al., 2005; Raasch and Harbusch, 2001; Shen and Leclerc, 1995; van Heerwaarden et al., 2014).

Because the impacts of surface heterogeneity on the ABL can occur on smaller spatial scales than the ones explicitly resolved by regional and global weather models, sub-grid cell heterogeneity is poorly represented. These impacts are represented either by aggregating the land surface to create a composite surface that provides one flux to the atmosphere (e.g. parameter aggregation) or a tiled approach where non-interacting tiles of different land surfaces provide a flux to the lowest model level which blends in the atmosphere like as is done with ECMWF's ERA5 reanalysis model (Bou-Zeid et al., 2020). In the latter method, the blending height is a useful concept for describing how the impacts of surface heterogeneity are projected in the ABL. Unlike the physical processes of the internal boundary layer and secondary circulations, blending height is a concept that arises from the practical need that our theory and numerical models necessitate a homogeneous surface. For example, in global scale numerical models, impacts of sub-grid scale surface heterogeneity blend to a composite ABL below the lowest grid cell of the model (Bou-Zeid et al., 2020). In this study, we define blending height the same as Mahrt (2000) where it is a scaling depth that describes the decrease of surface heterogeneity effects on the atmosphere with height. It is not necessarily a physical level where heterogeneity is no longer discernible, instead it is a threshold where the heterogeneity becomes negligible compared to a homogeneous case in the perspective of researchers.



Previous studies that have focused on the array of ways that surface heterogeneity can impact the ABL, have been either (1) observational studies which capture the realistic surface heterogeneities' impact on the ABL on a limited spatial scale or (2) idealized large-eddy simulation (LES) and direct numerical simulation (DNS) studies which create scaling theories to study how the heterogeneity can impact the ABL. Observational studies capture the realistic surfaces and heterogeneities, but typically measurements are unable to capture the full extent of the processes that govern the ABL response to the surface heterogeneity. Some examples of observational studies in heterogeneous areas include the LIFTASS-2003 Experiment (Beyrich and Mengelkamp, 2006), the CHEESEHEAD experiment (Butterworth et al., 2021) and the GRAINEX experiment (Rappin et al., 2021). While the observational studies focus on a relatively small spatial scale, another class of studies focus on idealized large-eddy simulations to write "textbook" cases of how surface heterogeneity impacts the ABL. There have been a few studies using realistic or real surface in LES including Hechtel et al. (1990); Huang and Margulis (2009) and Maronga et al. (2013). Because the impact of the surface heterogeneity on the ABL depend on the scale and strength of heterogeneity and the stability, it is unknown how and when these features of surface heterogeneity impact the ABL dynamics over the course of a realistic unstructured heterogeneity on a convective day.

The purpose of this study is to evaluate the impacts of surface heterogeneity on the ABL across three scales of heterogeneity over a representative LIAISE day both from a data-driven approach with the comprehensive LIAISE field campaign and modeling-driven approach with a high resolution LES. In this way, we can evaluate both the physical nature of how the surface heterogeneity impacts the ABL and the potential impacts of how resolved turbulence blends the heterogeneity with height in the atmosphere. Our approach is that we will start by exploring the LIAISE boundary layer development spatially (horizontal and vertical) and temporally (a composite typical LIAISE diurnal cycle) by combining a network of surface energy balance stations, radiosondes and aircraft data (Section 2). Because observations are limited in space and time, we employ LES to study how the ABL forms across spatial scales. But first, based on what we learn from the data, we will define more explicit sub-research questions to be explored with LES (Section 3). With the LES run using all the available data to be a realistic presentation of the LIAISE surface conditions and large scale ABL forcing, we will explore these sub questions (Section 4). In the discussion section (Section 5) we will bring model and data results together to come to an answer of the aforementioned general research question and the more explicit sub-questions posed in Section 3.

## 2 The LIAISE Experiment

The LIAISE field experiment took place between April and October 2021 in the Ebro River Valley in Catalunya in Northeast Spain with an intensive observation period (IOP) occurring in July 2021 (Boone et al., 2021; Mangan et al., 2023a). In particular, we focus our study on a period of three days in the middle of the IOP, 20-22 July 2021. The extent of the LIAISE experiment was characterized by a thermal surface heterogeneity due to locally applied irrigation in agricultural fields. Although the atmospheric conditions observed in the LIAISE experiment are controlled in part by the surface heterogeneity, there is strong coupling between the synoptic and mesoscale atmosphere and the regional scale land surface that complicate the dynamics of the ABL. For that reason, we selected these days with relatively weak synoptic forcing.

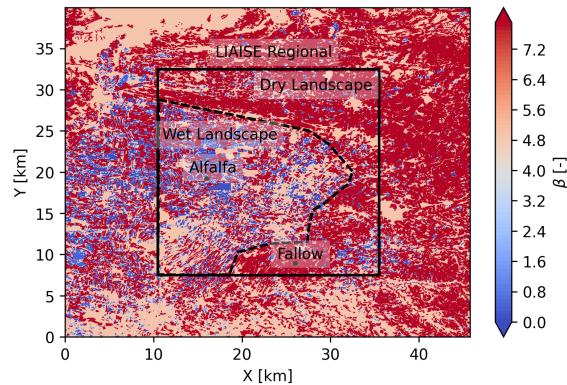


**Figure 1.** The observed surface Bowen ratio at 12 UTC in domain of the LIAISE LES. The spatial scales are indicated on the map with “LIAISE Regional” (bounded box), “Wet Landscape”, “Dry Landscape” (dashed line), “Alfalfa Local” and “Fallow Local” (points).

During the three day period, there was a thermal low building to the west of the LIAISE domain, which was influential in controlling the surface winds and the boundary layer development. Fig. 1 has the observed Bowen ratios ( $\beta \equiv H/LE$ ) for the extent of the LIAISE experiment at 12 UTC averaged over 20-22 July 2021 (Mangan et al., 2023a). In the irrigated area (west side of the domain),  $\beta$  are as low as 0.01, and in the rainfed area (east side of the domain)  $\beta$  are as high as 20. The difference  
95 in crop type and irrigation causes a strong heterogeneity with a length scale on the order of 10 times the ABL height, so one would expect a strong influence of this heterogeneity on the ABL.

## 2.1 Relevant Spatial Scales

There are a number of relevant spatial scales of surface heterogeneity that influence the atmospheric flow in the LIAISE domain. The largest scale of influence is the synoptic scale, which is important for controlling the mean wind and subsidence  
100 around our study area. The selected days of study, 20-22 July, are characterized by the development of a thermal low in the north center of the Iberian Peninsula to the west of the study area (Hoinka and Castro, 2003). In addition to the thermal low, in the late afternoons, the LIAISE area is also influenced by a sea breeze from the Mediterranean Sea (Jiménez et al., 2023; Lunel et al., 2024b). In the end of the afternoon, a cool and moist easterly wind reaches the LIAISE region, suppressing the ABL growth. Depending on the location of the thermal low, it can enhance or diminish the strength of the sea breeze.

105 Although these synoptic and mesoscale features define the environment, the ABL is also influenced by smaller spatial scales. We focus our study on the three scales of spatial heterogeneities as defined by Mangan et al. (2023a) and Mangan et al. (2023b): the LIAISE Regional scale, the Wet and Dry Landscape scales and the Alfalfa and Fallow Local scales (indicated in Fig. 1). The regional scale ( $\sim 10$ s km;  $\sim 10$  ABL height [ $z_i$ ]), which was the largest defined, is characterized by both the irrigated and the non-irrigated areas. It is the area of a single ERA5 grid cell. Within the regional scale, there are two landscape scales  
110 ( $\sim 1$  km;  $\sim 1$   $z_i$ ): the wet and dry landscape scales. Each landscape scale consists of the irrigated and rainfed areas and are characterized by the heterogeneity that arises between fields due to agriculture type and irrigation schedule. The separation





between the wet and the dry landscape scales is shown with the dashed line in Fig. 1. The smallest scale defined is the local or field scale consisting of homogeneous individual fields ( $\sim 100$  m;  $\sim 0.1z_i$ ), the irrigated alfalfa and rainfed fallow fields where much of the measurements were taken. These scales are shown by points in Fig. 1.

## 115 2.2 LIAISE Data

During the intensive observation period in July 2021, there were high spatial and temporal resolution of measurements of the land surface and the ABL. The surface and surface layer observations came from a network of surface energy budget stations in nine of the predominant crop types in the LIAISE domain. The fluxes from each SEB station was applied to a high-resolution crop-cover map to create spatial estimates of fluxes in the LIAISE regional domain. In addition to SEB  
120 stations, Catalunya has a dense network of automated weather stations operated by Servei Meteorològic de Catalunya (<https://www.meteo.cat/observacions/xema>). The stations around the LIAISE domain were used to estimate advection of temperature, moisture and wind using 10 m wind and 2 m temperature and humidity measurements. Both the flux maps and the advection calculation are described in more detail in Mangan et al. (2023a). The extent of the surface layer was studied by two 50 m  
125 towers: one located in an irrigated alfalfa and one in a non-irrigated fallow field. These 50 m towers included sensible heat flux measurements at 3, 10, 25 and 50 m and latent heat flux at 3 and 50 m. Furthermore, the 50 m towers each measured wind, temperature and humidity in a profile.

In addition to the surface and surface layer observations, there were a number of measurements of the ABL located in both the alfalfa and fallow fields. During the IOP, hourly radiosondes were launched at each site between 06 and 18 UTC. Furthermore, there was a tethersonde in the alfalfa field which was repositioned vertically approximately hourly during the  
130 daytime. Typically, the tethersondes measured turbulent fluxes including that of moisture and buoyancy between 100 and 500 m AGL at a time resolution of approximately 30 minutes. Finally, the SAFIRE aircraft measured turbulent fluxes of buoyancy, moisture and momentum in the ABL once per day during the IOP (Brilouet et al., 2021). The measurement strategy included flying “legs” each over the irrigated and non-irrigated areas at heights from 600 – 2000 m AGL and a transect across the wet-dry transition between the alfalfa and fallow fields at approximately 1500 m AGL. On all days, the aircraft flew between  
135 12:00-16:00 UTC.

We have chosen to use a composite “golden day” in this experiment to maximize the data usage. Because the observations are not all continuous in time, by combining multiple days over the afternoon period, we can create a composite dataset that is more representative of the variability of the atmosphere in the afternoons. The golden day is composed of three days – 20-22 July – which are characterized by the thermal low which developed in the north-central area of the Iberian Peninsula. Note that  
140 in all cases, all processing and normalization was done on individual observations before aggregating to create the golden day.

## 2.3 Observed ABL from LIAISE Experiment

Boundary layer observations from the composite golden day show the diurnal evolution of the boundary layer potential temperature and specific humidity profiles in the wet and the dry landscapes of the LIAISE campaign (Fig. 2). In the morning, between 8 and 10 UTC, we observe stable profiles in both landscapes. Temperature differences between the irrigated and non-

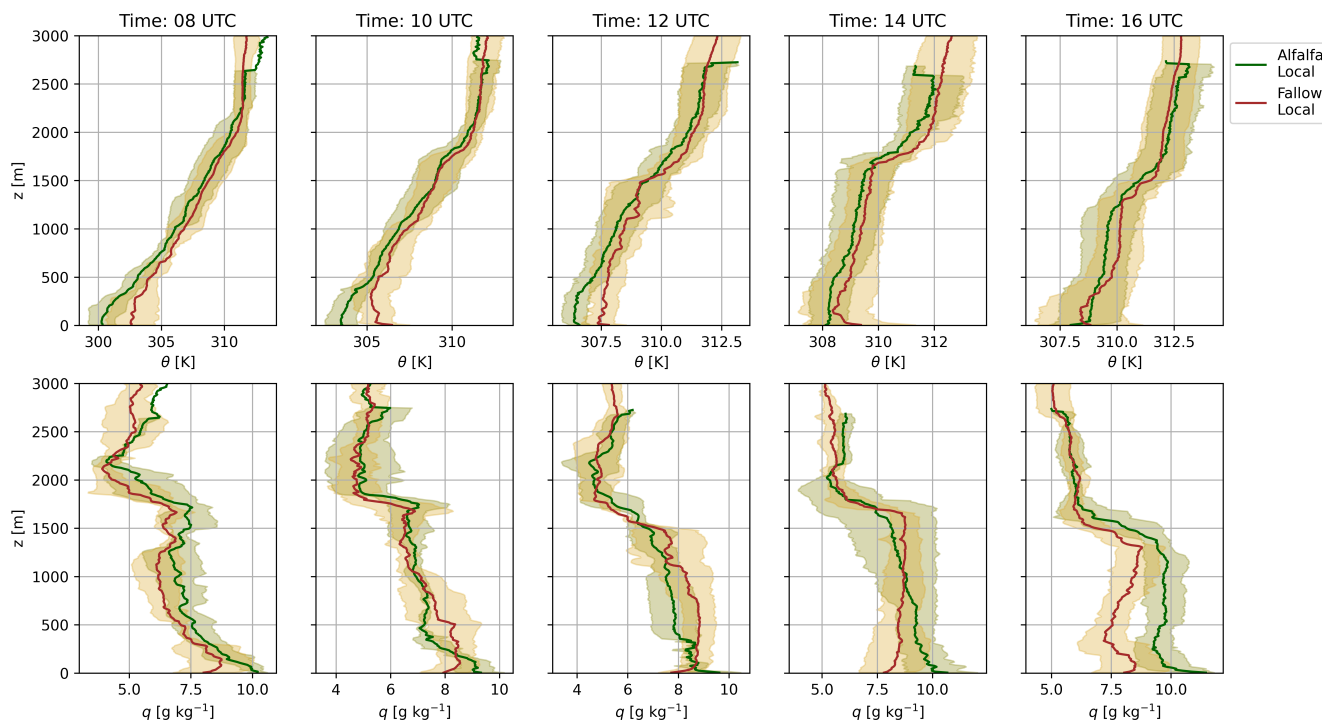


**Figure 2.** The radiosondes launched at the alfalfa field (green) and the fallow field (gold) on averaged over 20-22 July 2021 at 8, 10, 12, 14 and 16 UTC. The top panels are the potential temperature profiles, and the bottom panels have the specific humidity profiles.

145 irrigated profiles are small above 1 km; however, even by 10 UTC, we observe a wetter surface layer from the wet profile than the dry profile. At 12 UTC, the well-mixed convective boundary-layer begins to form. In the wet area, there are two distinct well-mixed layers in the temperature profile: one from the surface to 500 m, and one between 500 m and 1000 m. This layering is not apparent in the humidity profile. The layering in the wet landscape radiosonde data continues in the afternoon at 14 UTC, while the dry landscape radiosonde data show a traditional single well-mixed profile. Moreover, there is a strong signal of either  
150 entrainment or advection in the humidity profiles as the specific humidity in the wet area decreases with height towards the top of the ABL. This could be connected to the presence of a secondary circulation which could increase entrainment as shown by van Heerwaarden and Vilà Guerau de Arellano (2008). By the end of the afternoon, at 16 UTC, the sea-breeze arrives at the LIAISE region. The surface temperature cools in both locations, but the remainder of the profile is well-mixed.

The radiosondes show the influence of the footprint on the observation. Near the surface, the profiles show more extreme  
155 gradients: unstable layers near the surface in the dry area and moist, internal boundary layers in the wet area. However, the profiles show similar mean values near the top of the ABL. This suggests that there is some sort of “blending height” for the conserved variables potential temperature and specific humidity between the wet and the dry areas within the ABL. Previous LIAISE studies hypothesized this “funnel” type of ABL where near the surface, observations are linked to local fields and near the top of the ABL, observations represent a composite of both the wet and dry areas (Mangan et al., 2023a).

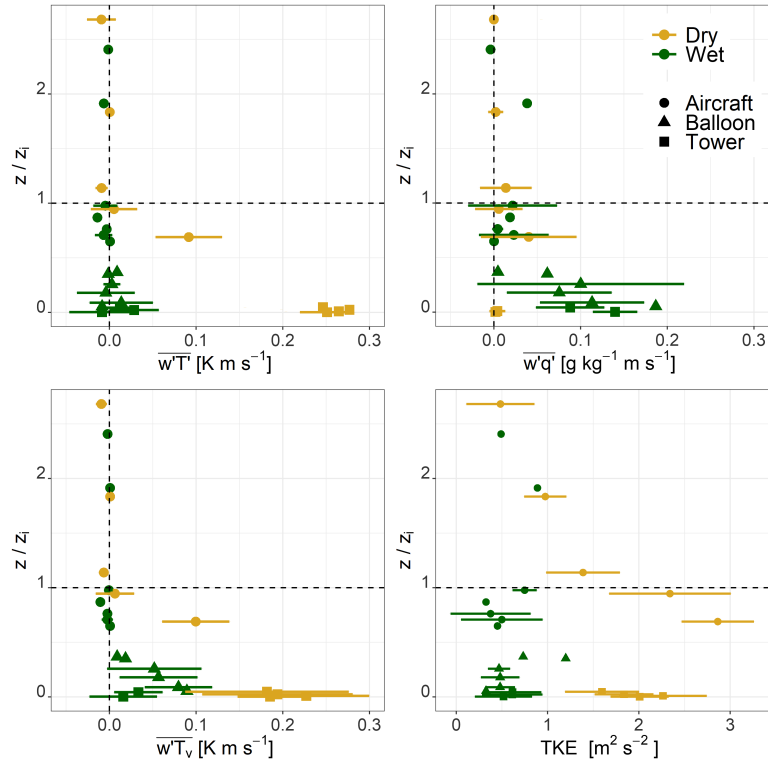


**Figure 3.** Composite flux profiles constructed at the alfalfa site (green) and the fallow site (gold). The vertical height is normalized by the boundary layer height ( $z_i$ ) from the radiosondes. The profiles are constructed using data from 20-22 July 2021 from 13:00 – 16:00 UTC. (a) The kinematic heat flux, (b) the moisture flux, (c) the virtual potential temperature (e.g., buoyancy) flux, and (d) the turbulent kinetic energy.

160 In addition to scalar profiles of the ABL from radiosondes, there were a number of different methods to measure turbulent fluxes within and above the ABL. Fig. 3 shows profiles of turbulent fluxes of heat, water vapor, buoyancy and turbulent kinetic energy (TKE) in both the wet and the dry areas. The profiles are normalized by the ABL height ( $z_i$ ) derived from the parcel method using the potential temperatures from the radiosondes (Kaimal and Finnigan, 1994). The observations are averaged both over the three composite days and the hours 13-16 UTC to create the composite profile. Although averaging the observations  
 165 over both the afternoons and with time could introduce errors, we assume that because each observation is normalized by observed  $z_i$  for each time individually that the scaling is reasonable for a convective ABL although the surface fluxes may differ. The standard deviation, which is shown with the error bars in Fig. 3, provides an indication of the diurnal and inter-day variability in the observations.

In the dry landscape, the turbulent fluxes follow traditional textbook profiles of the convective boundary layer (Fig. 3). At  
 170 the surface, there is the strongest sensible heat flux and it decreases nearly linearly with height. This consistent with the quasi-steady state approximation for potential temperature in the mixed layer. Near the top of the ABL, the heat flux is near zero. Above the ABL, the heat flux is small. In the dry area, there is a weak moisture flux near the surface, but this decreases near



the top of the boundary layer. The combination of the negative heat flux and positive moisture flux near the top of the boundary layer are indicative of entrainment from the free troposphere. In this landscape, the buoyancy flux is dominated by the signature of the heat flux, and follows the prototypical convective ABL flux patterns (Lenschow and Stankov, 1986; Stull and Driedonks, 1987). These turbulent fluxes of scalars are driven by TKE. In the wet landscape, there is strong TKE throughout the column of the ABL. Near the surface, the TKE is driven by the horizontal velocity components ( $u'^2$  and  $v'^2$ ); however, near the top of the ABL where convective thermals are stronger, the turbulence is more isotropic. At the top of the ABL in the wet landscape,  $u'^2 \approx v'^2 \approx w'^2 \approx 0.5 \text{ m}^2\text{s}^{-1}$  and compared to in the surface layer where  $u'^2 \approx v'^2 \approx 0.5$  and  $w'^2 \approx 0.1 \text{ m}^2\text{s}^{-1}$ .

Conversely, in the wet landscape, the turbulent heat flux is near zero from the surface through the entire ABL (Fig. 3). Near the surface, the error bars are large and show that there is uncertainty in the sign of the heat flux. Although the heat flux is small, the moisture flux in the wet area is high ( $\sim 0.1 \text{ gkg}^{-1}\text{ms}^{-1}$ ) from the surface through the lower half of the boundary layer. Above this layer, the moisture fluxes are near zero before showing a slight increase near the top of the ABL. Unlike in the dry area, in the wet area, the buoyancy flux has a large contribution from the moisture flux. In the bottom half of ABL, the moisture flux accounts for 20-50% of the total buoyancy flux. At the surface where heat flux is negative, there is a positive buoyancy flux because of the contribution of moisture. The buoyancy flux peaks at about 25% of the boundary layer height. From there, it decreases to near zero by 50% of the boundary-layer height. The fluxes of scalars are small in part because the TKE is smaller than the dry area and remains constant through the ABL. Near the surface, the TKE is driven by shear, like in the dry area, albeit, the variances of shear terms are smaller than in the dry area. In the middle of the ABL, the majority of the TKE difference between landscapes arises from the variance in vertical velocity. The buoyant thermals in the wet landscape are weaker than in the dry landscape, so overall, the mixing of turbulence is weaker in the wet area than the dry area. Both the TKE and buoyancy profiles suggest that there is an internal boundary layer from the surface up until  $z/z_i = 0.5$  that is capped by a turbulent layer that stretches towards the ABL top.

Finally, the SAFIRE aircraft flew cross-sections between the wet and the dry areas at 1500 m above ground level during each afternoon on 20-22 July. In Fig. 4 we show the observed temperature perturbation (where the mean is taken across the entire leg) and the velocity scale defined as the square root of the instantaneous turbulent kinetic energy ( $uTKE = \sqrt{u'^2 + v'^2 + w'^2}$ ) as used in Mangan et al. (2022). The x-axis is the distance from the boundary between the wet and the dry landscapes where negative numbers are taken over the wet landscape and positive values are taken over the dry landscape. The data in Fig. 4 was taken on the flight on 22 July from 13:30 to 14:30 UTC before the arrival of the sea-breeze and with relatively high values of surface fluxes. The data is averaged over four cross-sections of the flight that cross between the wet and the dry landscapes, and data was binned by distance to the boundary for each individual transect before aggregation.

In the wet landscape, the potential temperature perturbations ( $\theta'$ ) vary between  $\pm 0.1 \text{ K}$ , and the standard deviation in  $\theta'$  is on the same order of magnitude. As the aircraft crosses into the dry landscape, the  $\theta'$  increases to between  $\pm 0.25 \text{ K}$  and the standard deviation also increases. In the dry landscape, there are temperature ramps which indicate strong buoyant activity. Likewise, the signal of  $uTKE$  shows that there is stronger turbulent transport in the dry landscape than the wet landscape. The peaks of the  $uTKE$  signal correspond with the temperature ramps, which again suggests that the thermals are responsible for the peaks in TKE in the dry landscape. In the transition between the wet and the dry landscapes, there appears to be a sudden

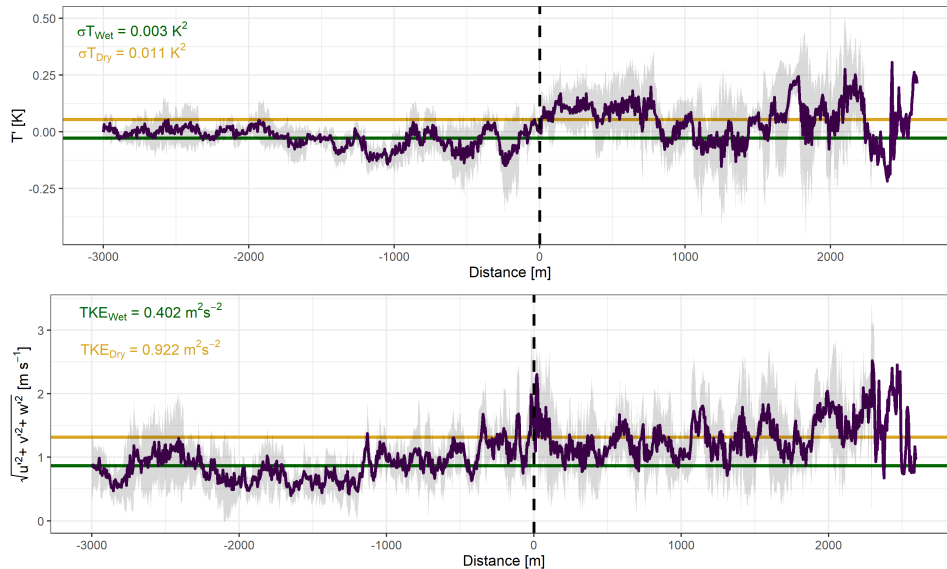


**Figure 4.** The transect from the aircraft flown at 22 July at 14:00 UTC. Negative distances on the x-axis are in the wet landscape and positive distances are in the dry landscape. The top panel is the temperature perturbations (with respect to the total transect) and the bottom panel is the square root of TKE for the same averaging time. The shading represents the standard deviation of these components averaged over four transects. The green and yellow lines indicate the average over the wet and dry landscapes respectively.

change in boundary layer characteristics. There is an increase in  $\overline{\theta'^2}$  and TKE in the wet landscape starting  $\sim 500$  m before the boundary.

### 210 3 Refined Research Objectives

To aid with explaining the conclusions from the observations and to prepare hypotheses for the LES experiment, we refer to Fig. 5 throughout this section.

From the observations, we note that above the dry landscape (right of Fig. 5), there is a prototypical, convective ABL throughout the day (Figs. 2 and 3). Profiles of potential temperature and specific humidity are relatively well-mixed, and  
 215 because of the warm surface, radiosonde profiles show superadiabatic lapse rates in the lowest hundreds of meters (Fig. 2, dry profiles in Fig. 5). Likewise, the flux profiles in the dry landscape show a typical linear decrease in height in the ABL (Fig. 3). However, there is some evidence that there is some influence of the wet landscape in the dry landscape: for example, there is an increase in moisture at the top of the ABL (Fig. 2 at times 8, 12, 14 and 16 UTC). Unlike the dry landscape, the wet landscape shows a layered, non-typical convective ABL (Fig. 2 and 3). In midday, the wet landscape radiosonde shows an IBL which is  
 220 evident through the potential temperature profile (Fig. 2) and there is a local peak in buoyancy flux at approximately 25-50% of the  $z_i$  (Fig.3). Above this zone, there is a turbulent layer (Fig. 3) that is well-mixed (Fig. 5). Because the observations are

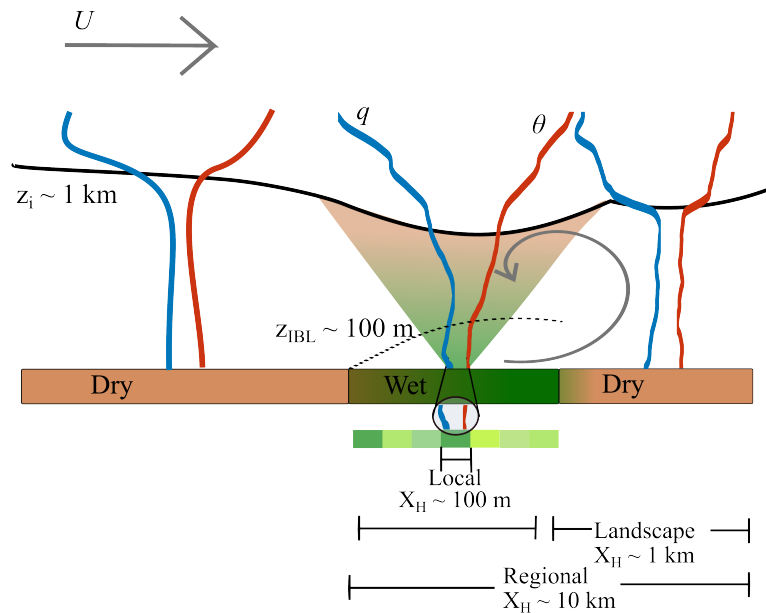


**Figure 5.** Schematic representation of the formation of the ABL (solid line, labeled as  $z_i$ ) in the LIAISE domain. An advective boundary layer from upwind moves over the wet landscape area where the ABL is modified with an internal boundary layer (dashed line, labeled as  $z_{IBL}$ ). The modified boundary layer is advected over the dry landscape where the convective turbulent motions eliminate the IBL.

located either in the wet landscape or the dry landscape, we cannot say much about the interactions between boundary-layers between the wet and dry areas with the observations alone.

While the observations are valuable for their high temporal resolution, the lack of spatial resolution makes it so we cannot answer the question of how these spatial scales of surface heterogeneity interact with each other to influence the ABL development. There are three related proposed ways that the surface heterogeneity impacts the ABL (in order from left to right in Fig. 5): an advective boundary layer, an internal boundary layer, and a secondary circulation. The interaction between these impacts are a function of spatial scale and wind speed. The advective boundary layer (indicated by the arrow labeled  $U$  in Fig. 5) indicates that the ABL could be formed upwind in a dry area, advected over the wet area where it is modified, and this modified ABL is then advected over the dry landscape. Advective boundary layers have been shown to be a defining feature in ABL dynamics in arid regions including in Chile's Altiplano Desert (Aguirre-Correa et al., 2023). In this way, the wet landscape can influence the dry landscape. Secondly, we observe a local IBL over the alfalfa field, however, from the observations, we can ask if the extent of the IBL extends over the entire dry landscape scale (IBL line, Fig. 5). Finally, because the observations occur mainly in two locations, it is not clear if there is a secondary circulation that forms because of the heterogeneity (curved arrow, Fig. 5). In this way, the dry landscape can influence the wet landscape.





To this end, we use a realistic large-eddy simulation to compliment the observations from the LIAISE campaign. Using an LES, we can connect the wet and dry landscape scales, so that we can study the impact of non-local processes on the development and dynamics of the atmospheric boundary layer. We can also explicitly investigate the development of the ABL at each of the relevant spatial scales of heterogeneity described in Section 2.1. We aim to address the following research questions with the LES experiment:

1. How does the interaction between the spatial scales impact the spatial development and diurnal cycle of the ABLs in the LIAISE experiment?
2. How do the scales of heterogeneity dynamically merge in the atmosphere in space and in height?

By addressing these research questions, we advance process-based understanding of how realistic unstructured heterogeneity influences a convective ABL and evaluate how numerical models can capture the turbulent transport from interacting heterogeneous patches.

#### 4 Large Eddy Simulation

We employ the MicroHH LES (van Heerwaarden et al., 2017) using large-scale forcing downscaled to the LES domain (van Stratum et al., 2023) from observations of advection (Mangan et al., 2023a). In this study, we prescribe surface fluxes measured during the LIAISE campaign to ensure a realistic distribution of heterogeneity in space (Mangan et al., 2023a). In Section 4.1, we describe the numerical simulation, and in Section 4.2 we show results for the ABL from the LES.

As our aim in using the LES is to study the impact of the surface heterogeneity on the development of the ABL, we selected the results shown to answer the aforementioned research questions. Therefore, we refer to Appendix A for validation of the LES compared with data from the LIAISE experiment.

##### 4.1 Model Configuration

MicroHH is a computational fluid dynamics simulation which supports direct numerical simulation and large-eddy simulation (van Heerwaarden et al., 2017). In this experiment, we employ the LES version of MicroHH at 30 m horizontal resolution over a domain of 39 km x 43 km centered on the LIAISE regional domain (Fig. 1). There are 196 grid cells in the vertical with a resolution of 25 m. This domain is large enough to allow the surface to be in equilibrium with ABL before reaching the inner LIAISE domain, while the resolution is fine enough to capture the field-scale processes. We use periodic boundary conditions with the large-scale forcing prescribed from observations. In this case, we use prescribed surface fluxes, and the surface layer model was based on Monin-Obkhov similarity theory with no slip conditions, and there was no radiation scheme. We selected the Smagorinsky sub-grid-scale parametrization with a fifth-order advection scheme.

We simulated a single composite day using the MicroHH LES between 6 and 18 UTC to represent the external forcing of the LIAISE golden day which comprises 20-21 July 2021 (Mangan et al., 2023a). We considered the first two hours of the simulation to be spin-up, so our analysis begins at 8 UTC. The initial profile of the atmosphere was prescribed using



the radiosonde launched in the dry landscape at 6 UTC. In terms of large-scale forcing, we have the option to prescribe (1) advection of potential temperature, specific humidity and wind into the domain ( $\vec{U}$  in Fig. 5), (2) geostrophic wind, (4) subsidence, and (3) nudging the domain mean towards observations. The advection terms for temperature, specific humidity and wind were calculated from observations from automated weather stations located in the larger LIAISE domain. See Mangan et al. (2023a) for details of the advection calculation. Although the advection terms were calculated using 10 m wind and 2 m temperature and humidity observations, the advection terms were prescribed at all heights in the LES domain. Mangan et al. (2023a) and Mangan et al. (2023b) show that the ERA5 reanalysis misrepresents the LIAISE domain because it misses both the irrigation and does not capture the correct location of the thermal low. For this reason, we opted to neglect geostrophic wind and subsidence. Finally, we nudged the domain averaged profiles of potential temperature, specific humidity and wind hourly to the radiosonde observations from the dry landscape scale.

Because in this study our focus is primarily the development of the ABL, we prescribe observed surface fluxes of sensible and latent heat fluxes and roughness lengths using the “flux map” product described by Mangan et al. (2023a). By prescribing surface fluxes from observations, we can focus directly on how the atmosphere feels a realistic surface. We are most interested how the boundary layer forms in this study, so it is beneficial to reduce the complexity of the coupled land-atmosphere system to consider only the one-directional impact of the surface on the atmosphere.

## 4.2 ABL Dynamics in a Realistic LES

In this section, we show the results of the realistic LES experiment. In Section 4.2.1, we analyze at the spatiotemporal evolution of  $z_i$  and characteristics. In this section, we consider how the ABL behaves at individual spatial scales. In Section 4.2.2, we shift the focus to study how the spatial scales interact with each other to influence the structure of the ABL. We evaluate spatial spectra of key parameters of the ABL development to study the relevant spatial scales. We consider how the ABL adjusts as it moves from wet to dry landscape scales. Furthermore, we introduce a criterion of blending height to investigate how spatial scales blend with height in the ABL.

### 4.2.1 Spatiotemporal Evolution of the ABL Across Spatial Scales

Using Figs. 6 and 7, we can identify the spatial (Fig. 6) and temporal (Fig. 7) variability in  $z_i$  across the spatial scales of the LIAISE domain. For the LES, we defined the boundary-layer height using the parcel method based on the near-surface air temperature (Stull, 1988) with a maximum jump in potential temperature of 0.25K to identify the top of the mixed-layer. We find that over the course of the day, the ABL grows faster in the dry area than the wet area (Fig. 6). In Fig. 6, the boundary layer height is highly variable in space as well. In the north-west corner of the irrigated area, the ABL height is the lowest, and it increases towards the southeast, increasing even in the wet landscape. In the irrigated region, the  $z_i$  is on average lower than the non-irrigated landscape. The difference is maximized near 12 UTC with a difference of 300 m (Fig. 7). However, although there is a mean difference between the wet and dry landscapes, the standard deviation within each of these scales is greater than the mean difference between them. The impact of individual fields on the local boundary layer height is greater than the total difference between the irrigated and non-irrigated landscapes. At the local scale, the ABL heights are more extreme,

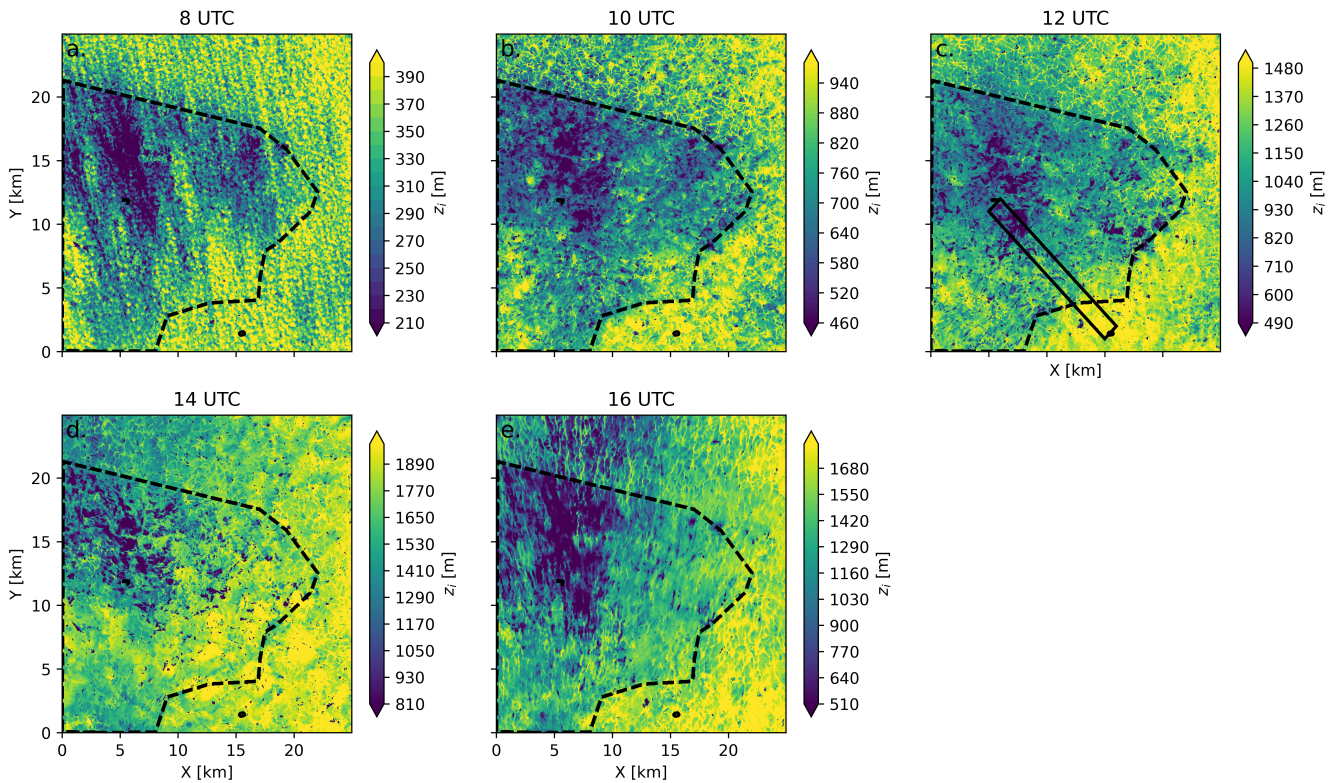


**Figure 6.** The ABL height at 8, 10, 12, 14 and 16 UTC calculated from the parcel method with a temperature jump of 0.25. The marked boundary is the difference between the irrigated and non-irrigated landscapes, and the points represent the alfalfa and fallow fields. The bounded box in panel (c) is the extent of the area used for the “adjusting ABL fluxes” from Fig. 10.

300 particularly regarding the morning growth of the ABL (Fig. 7), but when the sea-breeze arrives by the end of the afternoon ( $Adv_\theta = -0.3 \text{ Khr}^{-1}$  and  $Adv_q = -0.001 \text{ gkg}^{-1}\text{hr}^{-1}$ ), the local scales collapse like the landscape and regional scales.

In Fig. 8, we display the spatially averaged resolved turbulent fluxes of heat (top row) and moisture (bottom row) for all spatial scales. The dashed line indicates the combined resolved and non-resolved fluxes from the between the lowest grid cells and the prescribed surface flux. The y-axis is normalized by the mean boundary layer height at each scale. The fallow local scale has the highest heat flux from the surface and  $z/z_i \sim 0.5$  at all times of the day. All scales have the resolved heat fluxes decreasing linearly with height to the top of the ABL, like is seen with the observations in the dry landscape from Fig. 3. The heat flux is lower in the wetter scales than the drier scales. At the top of the ABL, the entrainment zone (as defined by a negative heat flux) occurs near  $z/z_i \sim 0.75$  and 1.25 at all times. For heat flux, the warm air entrainment is highest at the dry scales (fallow local and dry landscape) compared to the wet scales. Like Fig. 3, the alfalfa local scale shows the increase with heat flux between the surface and  $z/z_i \sim 0.3$  and weak entrainment fluxes above the  $z/z_i \sim 0.5$ . This signature is not evident in the wet landscape scale. This suggests that an IBL forms at the local scale and not across the entire landscape scale.

310

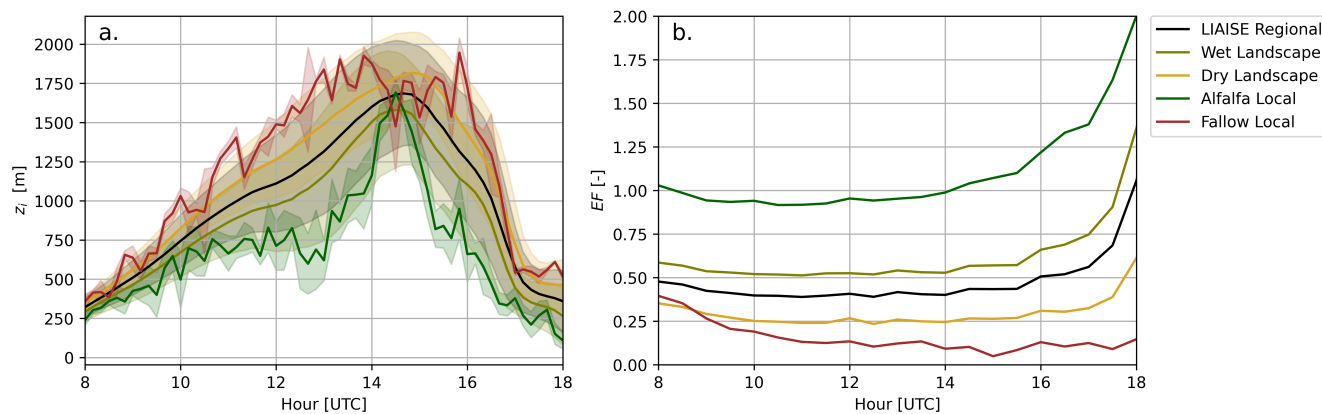


**Figure 7.** (a) The time series of the mean (solid line) and the standard deviation of boundary layer height for each spatial scale. (b) The mean evaporative fraction ( $EF \equiv LE/[H + LE]$ ) at each spatial scale from 08-18 UTC.

Concerning the moisture flux, the alfalfa local and the wet landscape scales provide much of the moisture for the entire domain. There strong flux diverge in moisture flux in both of these scales throughout the lower half of the ABL. In the dry scales, the moisture flux between the landscape and fallow local scales are similar and low in the bottom half of the ABL; however, unlike in the wet areas, there is a strong increase of moisture flux with height near the top of the ABL. This agrees with the observed moisture fluxes in Fig. 3. Near the top of the ABL, the entrainment of dry air from the free atmosphere leads to a strong moisture flux in the dry areas compared to the wet ones. Both the heat and moisture signals indicate stronger entrainment zones in the dry landscapes than the wet ones, which is likely a consequence of the higher  $z_i$  in these scales as shown in Fig. 7.

#### 320 4.2.2 ABL interactions among spatial scales

So far, we have only considered the different ABLs that arise at the spatial scales of heterogeneity introduced in Section 2.1. In reality, these ABLs are not separate: the atmosphere mixes the impacts of the surface heterogeneity. To look at how the ABL mixes across the spatial scales, we start by examining the two-dimensional spatial spectra of key variables that influence the ABL to determine their most representative length scales. This provides an indication whether the ABL reacts to the same scales of heterogeneity as the surface fluxes. Next, we study the same cross-section between the alfalfa and the fallow fields as Fig. 4 to study how the ABL adjusts as it crosses the wet-dry boundary. Finally, we apply a model-driven approach to quantify the blending height among the spatial scales.

##### *Spectral Analysis*

Although we have defined the relevant spatial scales in this research based on physical characteristics, we can check the importance of these scales on the development of the ABL by calculating the 2-dimensional spatial spectra of surface fluxes,

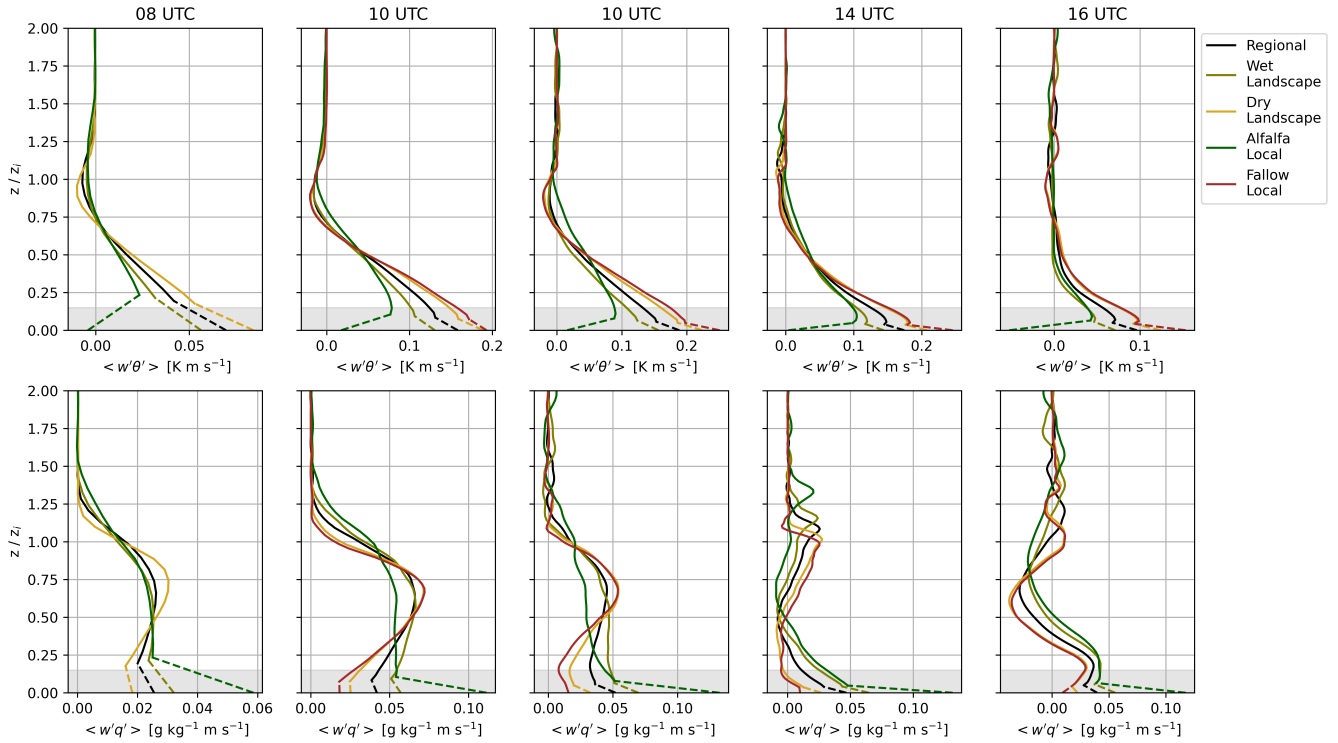


**Figure 8.** The profiles of LES resolved fluxes with height normalized by ABL height ( $z_i$ ) for each of the spatial scales. The shaded region indicates the surface layer. The dashed-line indicates the fluxes interpolated between the lowest resolved model level and the prescribed surface flux at each spatial scale.

vertical velocity and  $z_i$  (Fig. 8). Moreover, we define a characteristic length scale ( $\Lambda$ ) based on a weighted integral of the spectrum (Pino et al., 2006; de Roode et al., 2004):

$$\Lambda_\psi = \frac{\int_0^\infty S_\psi(k) k^a dk}{\int_0^\infty S_\psi(k) dk}; a \neq 0 \quad (1)$$

where  $\psi$  is a given variable,  $S_\psi(k)$  is the spectral density of the variance as a function of wave number  $k$ , and  $a$  is a weighing factor. Pino et al. (2006) describes their choice of  $a = -1$  to weigh the spectra towards the large-scale ranges, while Jonker et al. (1999) chose  $a = 1$  to weigh the length scale towards the smaller scales. We have selected to use  $a = -0.8$  for both the surface fluxes and  $z_i$  to better capture the mesoscale peak in the spectra, while  $a = -1$  was best for the vertical velocity to capture the larger scales.

Fig. 9 shows the results of the spatial spectra at 12 UTC for (a)  $z_i$ , (b) sensible heat flux, (c) latent heat flux, and (d) vertical velocity at 50% of the mean  $z_i$  (which was 1111 m at 12 UTC). The sensible and latent heat flux spectra are from the prescribed boundary conditions. The gray line indicates the weighted characteristic length scale. Both the surface fluxes and the  $z_i$  show



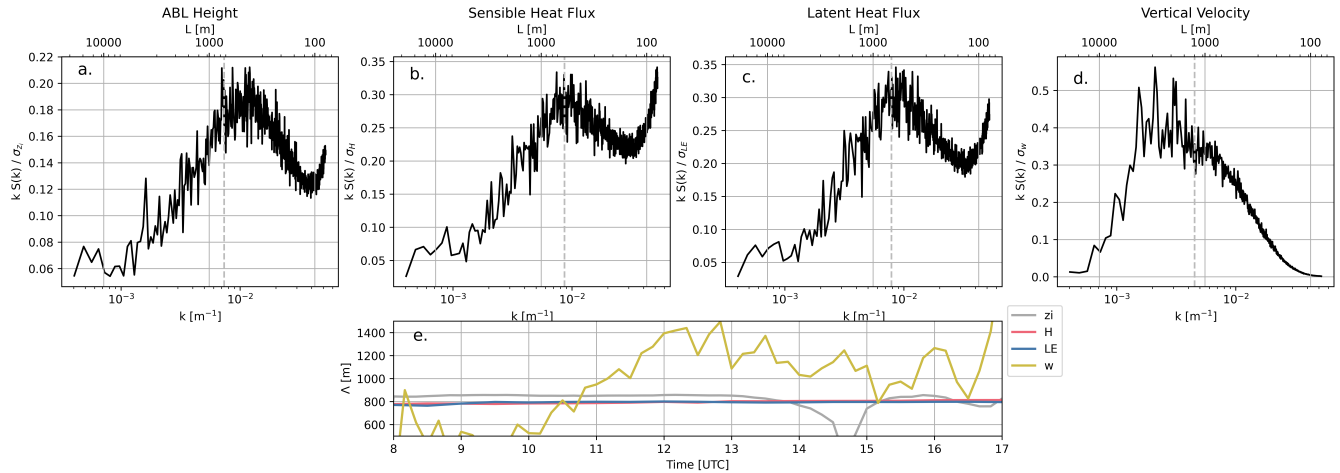


**Figure 9.** Spatial spectra of (a)  $z_i$ , (b) surface sensible heat flux, (c) surface latent heat flux, and (d) vertical velocity at 50% of the mean  $z_i$ . (e) is the integral length scale calculated with Eq. 1 over time in UTC.

bimodal peaks in the spectra: one with an integral length scale of approximately 800 m, and one in the microscale with a length scale of less than 100 m. The microscale peak relates to the differences between individual fields. This indicates that the ABL responds directly to the variability in fluxes from individual fields, although this effect is dampened as is evident in the reduction  
 345 in  $z_i$  variability in the microscale. This microscale peak in  $z_i$  indicates the presence of local IBLs with characteristic length scales of  $\sim 80$  m. The mesoscale peak in these signals indicates that within the landscape scales, there is a strong variability in both surface fluxes and  $z_i$ . This indicates that there may be a scale between the landscape and local scales that is most important for driving the ABL growth at the regional level.

Unlike the surface fluxes and  $z_i$ , the spectra of the vertical velocity shows more classical with a single peak in the mesoscale  
 350 range, with a length scale on the order of 1 km. This means that by 50% of the mean regional  $z_i$ , the surface fluxes aggregate to a circulation on the order of 1 km. This relates to the same order of magnitude as the landscape scales as previously defined. Because there is little variation in the microscale spectra of vertical velocity unlike that of  $z_i$ , the variability of  $z_i$  in the mesoscale may be representative of an IBL, but these impacts do not reach up to the level of 50% of  $z_i$ .

Over the course of the day, the integral length scales for surface latent and sensible heat fluxes are unchanging (Fig. 9e). The  
 355 length scale is approximately 800 m for both variables. This indicates that the sensible and latent heat fluxes are covarying, and although the evaporative fraction of different surfaces vary over the day (Fig. 7), the ratio between LE and H stays consistent. Like the surface fluxes, the  $\Lambda_{z_i}$  is constantly  $\sim 800$  m over the day, except for a brief dip between 14 and 15 UTC where the sea-breeze arrives in the domain and lessens the length scale. Finally, the  $\Lambda_w$  is the only variable to show a diurnal cycle. In the morning,  $\Lambda_w$  is  $\sim 500$  m and it increases to over 1 km in midday. When the sea-breeze arrives at the end of the afternoon,  
 360  $\Lambda_w$  decreases again to  $\sim 1000$  m. The time-varying  $\Lambda_w$  relates to the strength of the buoyancy-induced turbulent transport and has implications for the mixing between spatial scales.



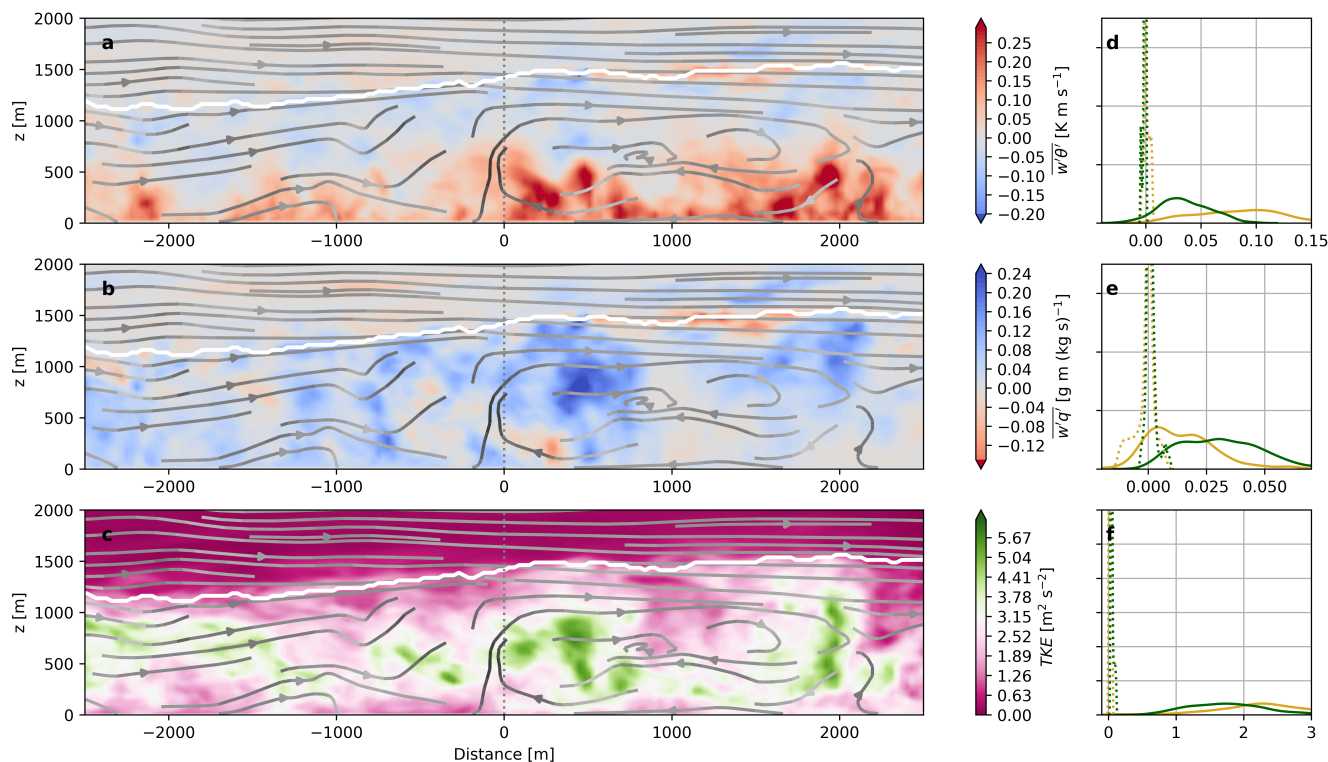


**Figure 10.** Transect from the wet landscape (negative) to the dry landscape (positive distances) from the LES. (a) The heat flux, (b) moisture flux and (c) turbulence kinetic energy averaged over individual transects that mimic the aircraft strategy. Panels d-f are the probability distributions of the fluxes from the wet landscape (green) and dry landscape (yellow). The entrainment fluxes are shown in the dashed lines and the surface-layer fluxes are shown in the solid lines. The streamlines in panels a-c are composed of the along transect wind component and the vertical velocity.

### Adjusting ABL

In Fig. 10, we show the instantaneous cross-section of the LES domain between the alfalfa field and the fallow field at 12 UTC. The negative distances indicate the wet landscape, and the positive distances indicate the dry landscape. The transect is computed from the box in Fig. 6a that runs from the northwest to the southeast in the LIAISE regional domain (315° from north). At this time, the wind speed above the ABL is approximately 2 ms<sup>-1</sup>, and the wind direction is predominantly from the west. Fluxes are calculated spatially over 50 transects that run parallel to the aircraft transects. The top panel is the heat flux, the middle panel is the moisture flux, and the bottom panel is the TKE. The streamlines indicate the along-transect wind direction ( $U$ ) and the vertical velocity. The panels on the right are the probability distribution functions (PDF) of the fluxes in the wet and dry landscapes respectively. The solid lines are fluxes from the surface layer ( $z/z_i < 0.15$ ) and the dotted lines are from the entrainment zone ( $0.75 z/z_i$  and  $1.25 z/z_i$ ).



Between the wet and dry landscapes, there is an increase in  $z_i$  along the transition between the wet and the dry landscapes of 400 m. Although the transition between the wet and the dry landscape scales is marked at 0 distance, the ABL responds to the dry landscape near the transition of the wet landscape. This is evident by the strong updrafts within the first 500 m of the transition. Comparing this result to that of Fig. 4 indicates that the aircraft may have been flying above the ABL in the wet landscape then enters it near the transition to the dry landscape. The sensible heat flux near the surface increases in the dry landscape, while the moisture flux decreases. TKE appears to be higher in the dry landscape than the wet as well, however, TKE is concentrated heavily in thermals, which are more prevalent in the dry landscape. Near the middle of the ABL, the heat flux weakens, while the moisture flux increases in the wet landscape. Like Fig. 4, TKE and convection are higher in the dry landscape than the wet landscape.

The PDFs of the fluxes confirm that in the surface layer, the heat flux is higher in the dry area than the wet area, and the opposite occurs with the moisture fluxes. In the surface layer, the TKE looks similar between the wet and the dry landscapes. The entrainment fluxes are more difficult to separate the impacts of the landscape scales. For the heat flux, the entrainment PDFs look similar: both distributions are centered around 0. For the moisture flux, it skews negative over the dry landscape and positive over the wet landscape. For both the heat and moisture flux, there is counter-gradient flux in the dry landscape. This could indicate the influence of the wet landscape on the ABL in the dry landscape. For TKE, there are pockets of strong TKE in the entrainment zone in the wet, although there is a skew to the highest TKE in the dry landscapes.

From Fig. 10, there is a weak secondary circulation that forms along this transect, and in approximately 1.5 km into the dry landscape, there appears to be a small circulation that is driven by relatively strong updrafts. Based on the wind speed, one a stronger secondary circulation could form in this region, however, it likely would be at a larger spatial scale than the regional scale. Furthermore, because of the averaging scheme to compute fluxes, impacts of IBL are smoothed in this figure. This confirms the results from Fig. 9 that suggests that IBLs form at the local scale instead of at the landscape scale.

### *Blending Height*

In addition to the physical processes that arise from surface heterogeneity, the concept of a “blending height” arises for both numerical modeling and observational applications. In both contexts, the “blending height” describes the height in which the surface heterogeneity is no longer noticeable. We consider the blending height to be a proxy of the strength of the mixing of state variable and turbulent moments that arises from the surface heterogeneity. There is no consensus of the definition of blending height in literature, instead it tends to depend on one’s purpose (e.g. model or observational considerations). In Fig. 10, we see that near the top of the ABL, the heat flux is not noticeably different between the scales, however, to quantify the areas in which the scales are blended, we use the coefficient of variation to determine the blending height, like Huang and Margulis (2009). The coefficient of variation ( $C_v$ ) is defined as

$$C_v \equiv \frac{\sigma_\psi}{\langle \phi \rangle}. \quad (2)$$

where  $\psi$  is any given variable and  $\sigma_\psi$  is its standard deviation in space and  $\langle \phi \rangle$  is its spatial mean. Huang and Margulis (2009) defined the blending height as the level in which the coefficient of variation for the heterogeneous case is less than or equal to that of the homogeneous case. However, a blending height can be defined relative to a number of dimensions including location,



height and domain. Therefore, in a general form, the blending height ( $B$ ) can be expressed as the ratio of  $C_v$  of dimension to that of another.

$$B(x, y, D, z) \equiv \left| \frac{C_{v,a}}{C_{v,b}} \right| \quad (3)$$

where  $x$  and  $y$  are locations in space,  $z$  is height and  $D$  is domain or model resolution. In its most general form, the blending height expresses the lowest level in the atmosphere where the surface heterogeneity is not felt by the atmosphere. In that case, the appropriate form of  $C_{v,b}$  would take the field averaged over the entire heterogeneous domain, while  $C_{v,a}$  would be the field as a function of height and domain. With this definition, we observe a local minima of  $B$  inside the ABL which represents a blending zone, and a local maxima of  $B$  in the entrainment zone corresponding to the entrainment processes which causes the atmospheric fields to be heterogeneous.

415 However, in this case, we are interested in the height where the where spatial scales blend together instead of the hypothetical case where the entire region is homogeneous. By comparing scales directly, we can study the impacts of the heterogeneity on grid size of a regional or global model. Therefore, we define the blended zone to be where the  $C_v$  of two scales are within 5% of each other. We found that the choice of threshold was not sensitive to the results of the blended zone. In effect, this method means that we consider scales to be blended if the normalized variability of a given variable are approximately equal.  
420 In specific form, the blending definition used in this study is

$$B(z|D) \equiv \left| \frac{C_{v,a|D_a}}{C_{v,b|D_b}} \right| \leq 0.05. \quad (4)$$

Because our scales are nested, we analyze at the heights in which the local scales (alfalfa and fallow) blend into their respective landscape scales (wet and dry) in Fig. 11a and 11b. We also can study where the landscape scales blend into the total LIAISE regional scale in Fig. 11c and 11d. In Fig. 11, we show a time series of the blending height from the surface (normalized by  $z_i$  for the smaller scale) for the scalars of potential temperature and specific humidity and the fluxes of heat and moisture for each of the scales. In general, we do not identify a strong diurnal cycle for these blending heights, and the lowest level of blending depends on the selected variable.

We assume that the blending occurs first from the surface up into the atmosphere first from the local scales to the landscape scales, and then from the landscape scales into the regional scale, so we use a bottom-up approach. The local scales blend into the landscape scales within or closely above the surface layer. At the fallow scale, the moisture flux blends between  $z/z_i = 0.3-0.4$  in the morning, while all other fluxes blend within the surface layer (less than  $0.15 (z/z_i)$ ). This indicates that the fallow local scale is relatively similar to the rest of the dry landscape scales except in the moisture flux. The alfalfa local scale blends at a higher height for potential temperature and heat flux than the moisture variables. Conversely, in the morning, the blending height for moisture terms is higher than those of the heat terms. When we compare this result to the flux profiles in Fig. 8, we observe that the wet landscape and alfalfa local scales, the moisture fluxes converge closer to the surface than the heat fluxes, and that between the dry landscape and fallow local scales, the heat fluxes converge closer to the surface than the moisture fluxes. This could suggest that the scales mix closer to the surface for variables which are more similar between scales; the dominant process for a given scale has a lower blending height.





(e.g. dry landscape). The transport may not be statistically different within and outside of thermals, but strong updrafts could push up the ABL top leading to more entrainment. Thereby, like the surface, the entrainment zone “de-blends” the flow in heterogeneous areas. We show an example of this in Appendix B.

## 5 Discussion

Surface heterogeneities can impact the ABL in a number of ways in vertically and horizontally in the ABL. In this study, we use the realistic case from the LIAISE campaign and a combination of observational and a numerical experiment using LES. In order to combine the methods, we first discuss the dynamics of the ABL across the spatial scales in Section 5.1. In Section 5.2, we shift our focus to the implications for how sub-grid scale heterogeneity is handled in numerical models.

### 5.1 ABL Across Scales

At the local scales – the alfalfa and fallow fields – we find that the land-surface scale is not large enough to impact the entire depth of the ABL. There is high variation in  $z_i$  and characteristics like temperature and humidity, which indicates the presence of localized IBLs at this scale. From observations, there is a clear IBL at the alfalfa local scale based on the layered potential temperature profile of the radiosonde and the flux regime in the bottom half of the ABL. At the alfalfa local scale, the surface layer becomes stable, but it is topped by a convective boundary layer (Fig. 2). The LES is able to capture the stable layer at this scale as evident through the flux profiles (Fig. 8). At the fallow local scale, there is not a clear IBL from either the observations or the LES because it is relatively warmer than the domain. Finally, the peak variability in this length scale in the spectra of  $z_i$  indicates that IBLs are formed at this scale, but do not cross defining the landscape scale.

The wet and dry landscape scales are characterized by the differences between fields of the irrigated and non-irrigated areas of the LIAISE domain. From the LES, we find that the mean  $z_i$  of the wet landscape is at most 300 m lower than that of the dry landscape. The spectral analysis of  $z_i$  shows that it varies most within the landscape scale ( $\Lambda_{z_i} \sim 800$  m). At the landscape scale, the variability in the height of the ABL is larger than the mean differences in the height of the ABL. This indicates that the local scales which make up the landscape scale are more variable within each landscape scale than between them. The local scales blend into the landscape scales within the surface layer of the ABL, so the impacts of individual fields do not impact the ABL above  $z/z_i \sim 0.3$ . In Fig. 10, we find that there is a gradual increase in  $z_i$  in a cross-section between the landscape scales, and TKE enhances the mixing in the dry landscape scale compared to the wet landscape scales. Finally, there is no evidence of secondary circulations within each landscape scale because the length scale of heterogeneity is smaller than the  $z_i$ . This agrees with findings from Patton et al. (2005).

The regional scale is characterized by the heterogeneity between the wet and dry landscape scales. We might expect a secondary circulation to occur within this scale based on the scale of the heterogeneity (Patton et al., 2005). In the LIAISE area, Lunel et al. (2024a) captured secondary circulations with a mesoscale model; however, there is not a strong influence of the secondary circulation in the LES. There are a few possible reasons for this. The first is the background wind. Hechtel et al. (1990) ran an LES with a realistic land surface and found no secondary circulation, which they suspected was due to the



485 high velocity in the domain. Avissar and Schmidt (1998) and Raasch and Harbusch (2001) found that a mean background wind  
greater than  $2.5 \text{ ms}^{-1}$  reduces the formation of secondary circulations if is not normal to the boundary. In our case, the wind is  
mainly westerly, while the boundary is curved. Additionally, because the pattern of the heterogeneity in this case is relatively  
unstructured in the landscape scale, its impacts are not felt as strongly as if they were structured. Our study differed from that of  
Lunel et al. (2024a) mainly because of the scale and the unstructured (i.e. each field has a different flux regime) heterogeneity.  
490 In this study, we focused on the extent of an ERA5 grid cell, while Lunel et al. (2024a) modeled all of Catalunya and found  
secondary circulations with length scales of  $\sim 100 \text{ km}$ . Furthermore, they used a coupled model where the soil moisture in  
the irrigated fields was at field capacity. In this study, we maintained the microscale heterogeneity that occurred within the  
landscape scale, which on a whole lessened the differences in surface fluxes between the wet and dry landscape scales.

Unlike the landscape scales, the blending height from the surface in the regional scale occurs between  $z/z_i$  0.3 and 0.8 in the  
495 mornings before the atmosphere is convective. During the afternoon convective period, the blending heights decrease below  
 $z/z_i = 0.2$  for potential temperature and the heat flux. However, moisture and moisture fluxes do not blend until near the top  
of the boundary layer even when the atmosphere has strong, convective mixing. Convective turbulence, which arises from the  
buoyancy flux, is responsible for controlling the blending height. Moreover, because the entrainment varies between the wet  
and dry landscapes, we observe that there is an “unblended” zone at the top of the ABL in the regional scale. This implies that  
500 although heterogeneity arises from the surface, its impacts are felt through the entire ABL.

## 5.2 Implications for Handling Sub-grid Heterogeneity

In our study, we focus on the variety of physical processes that control the dynamics of the ABL. Despite our focus on  
process understanding, the results of this study could have implications how sub-grid scale heterogeneity is handled in regional  
scale weather models. Sub-grid scale surface heterogeneity is often handled either with the parameter aggregation approach  
505 or with the flux aggregation approach. In the parameter aggregation method, the land surface is linearly averaged over the  
heterogeneity. Mangan et al. (2023a) and Mangan et al. (2023b) use a parameter aggregation method to represent the LIAISE.  
Conversely, in this study, we explicitly resolve the surface in the LES, which allows the atmosphere to mix out the impacts of  
the heterogeneity, which allows this approach to be a proxy flux aggregation approach.

Mangan et al. (2023a) found that the parameter aggregation over the regional and landscape scales re-created the dynamics  
510 of the ABL from the observations. This suggested that the regional ABL was formed through a combination of the land surface  
from both the wet and dry areas. In this study, where scales are able to interact in the atmosphere, we notice similar results:  
the difference in the  $z_i$  between the regional scale is comprised as a composite of the landscape scales, and its impacts are  
relatively linear. Individual fields have little impact on the regional scale; however, collectively, the relatively wet and dry  
landscape scales begin to impact the regional scale.

515 In these cases, the regional scale represents a single grid cell of a global model, and the selection of the landscape and local  
scales represents possible future model resolutions where the sources and strength of sub-grid scale heterogeneity differs. At  
the resolution of regional scale, flux aggregation occurs at approximately  $z/z_i \sim 0.5$ , however, it varies depending both on  
the variable and the atmospheric stability. The differences in fluxes in the entrainment zone should be taken into account in





order to better capture the impacts of the surface heterogeneity on the ABL. We use the landscape scales as a proxy for higher  
520 resolution models. We find that the differences between flux profiles and ABL height are more notable between landscapes  
than between fields. From the surface, the blending between the local and landscape scales occurs in the surface layer, so the  
aggregation occurring near the surface is more reasonable at this resolution.

## 6 Conclusions

By combining surface and upper air observations of mean and flux state variables of the ABL with a high resolution, realistic  
525 LES, we study the dynamics of the ABL. Particular emphasis is placed how these dynamics are acting across different spatial  
scales driven by a very large surface heterogeneity with characteristic length scales. The observations show the presence of an  
IBL locally in an alfalfa field where buoyancy flux at the surface is solely driven by the moisture flux. In contrast a prototypical  
convective ABL in the fallow field. We hypothesize that there are interactions between the irrigated and non-irrigated areas  
which influence the dynamics of the ABL. Our main findings are the following:

530 1. *How does the interaction between the spatial scales impact the spatial development and diurnal cycle of the ABLs in the  
LIAISE experiment?*

The local scales, which are characterized by individual fields, are driven by extreme surface fluxes ( $\beta < 0.1$  and  $\beta > 20$ ).  
Internal boundary layers form at this scale over the course of the day, but they do not persist at the larger scales. Because of  
the relative size of the local scale ( $\sim 100$  m) compared to the  $z_i$  ( $\sim 1000$  m), the impact of the local scale on the total ABL is  
535 relatively limited. Therefore, we find in both the model and observations a stable surface layer topped by a convective boundary  
layer in the alfalfa local scale. At the landscape scales, the heterogeneity arises from individual fields within the irrigated or  
non-irrigated areas. The variability of the ABL within the landscape scales is much larger than the differences among the scales,  
therefore, our findings show that there is no IBL that forms within or between the landscape scales. From the LES numerical  
experiments, both landscape scales (wet and dry) show a prototypical ABL, although buoyancy is weaker in the wet landscape  
540 than the dry landscape. Finally, at the regional scale heterogeneity is formed by the contrast of irrigated and non-irrigated  
agricultural fields. The regional ABL characteristics fall between the extremes of the two landscape scales, which could be a  
function of the strong vertical mixing that arises from the dry landscape scale.

2. *How do the scales of heterogeneity dynamically merge in the atmosphere in space and in height?*

Based on spectral analysis of the LES results, we observe that the length scale of the ABL height follows that of the surface  
545 fluxes. There is peak variability in ABL height in the mesoscale ( $\Lambda_{z_i} \sim 800$  m) which relates to the landscape scale and the  
microscale ( $\sim 100$  m) which confirms that IBLs are formed at the local scale. By analyzing the blending height from the LES,  
we discover that the local scales blend into the landscape scales by  $z/z_i = 0.3$  for scalars and turbulent fluxes under convective  
conditions. The landscape scales blend into the regional scale by  $z/z_i = 0.8$  for scalars turbulent fluxes under convective  
conditions. The blending height depends on the variable of interest as well and the strength of the buoyancy of the turbulence.



550 Because the strength of entrainment is higher in the dry landscape than the wet landscape, there is a second, unblended layer in the entrainment zone above  $0.8 z/z_i$ . The role of entrainment fluxes on blending within the ABL should be taken into account in weather models to better capture the impacts of surface heterogeneity on the ABL.

Increasing our understanding of how surface heterogeneity impacts the dynamics of the ABL in a realistic case is an important step in understanding the full impacts of surface heterogeneity on the bi-directional land-atmosphere interactions. In the  
555 LIAISE domain, the local field scales mix into the landscape scales close to the surface, while the impacts of the landscape scales are felt throughout the depth of the ABL and with a horizontal length scale  $\sim 800$  m. Because of the patchy surface representation and a maximum background wind of  $2 \text{ ms}^{-1}$ , the impacts of secondary circulations are not felt as clearly as previous idealized LES studies suggest (e.g. Patton et al. 2005; van Heerwaarden and Vilà Guerau de Arellano 2008). Finally, by  
560 combining observations with an LES case study, we confirm that the increased buoyancy flux from the dry landscape influences the state variables observed in the wet landscape.

*Code and data availability.* In-situ observations from the LIAISE field experiment can be found on the LIAISE catalog: <https://liaise.aeris-data.fr/>. The MicroHH LES code can be found at <https://github.com/microhh/microhh>, and its documentation can be found at <https://microhh.readthedocs.io/en/latest/index.html>. The statistics from the LES experiment as well as the input data is available for download at <https://doi.org/10.5281/zenodo.13379335>.

## 565 **Appendix A: Validation of LES experiment**

We performed sensitivity studies for this LES experiment with the large-scale forcing components. In Fig. A1 we show the results of the spatial means of potential temperature and specific humidity for the LES scales compared to the radiosondes with LIAISE observations. We expect the radiosondes to best represent the wet and dry landscape scales. The shading represents the standard deviation of the observations averaged over the LIAISE golden days.

570 In our selected case, the LES captures the approximate ABL height compared to the radiosondes for both the wet and the dry landscapes. In the afternoon, there is a warm bias compared to the radiosondes at all scales, but moisture appears to be well captured. Furthermore, the spread between the wet and dry landscape scales in the model is less than with observations. This is likely due to the surface representation and the assumptions used as we were able to capture the observed wind using the observationally-driven large-scale forcing terms.

## 575 **Appendix B: Blending Height**

Because blending height was computed spatially, we can observe the “blending region” in the ABL using a time-height figure. Fig. B1 shows an example of the “blended zone” from the wet landscape to the LIAISE regional scales for (a) potential temperature, (b) specific humidity, (c) heat flux, and (d) moisture flux. The gray indicates the blended zones (where  $\left| \frac{C_{v,wet}}{C_{v,dry}} \right| <$

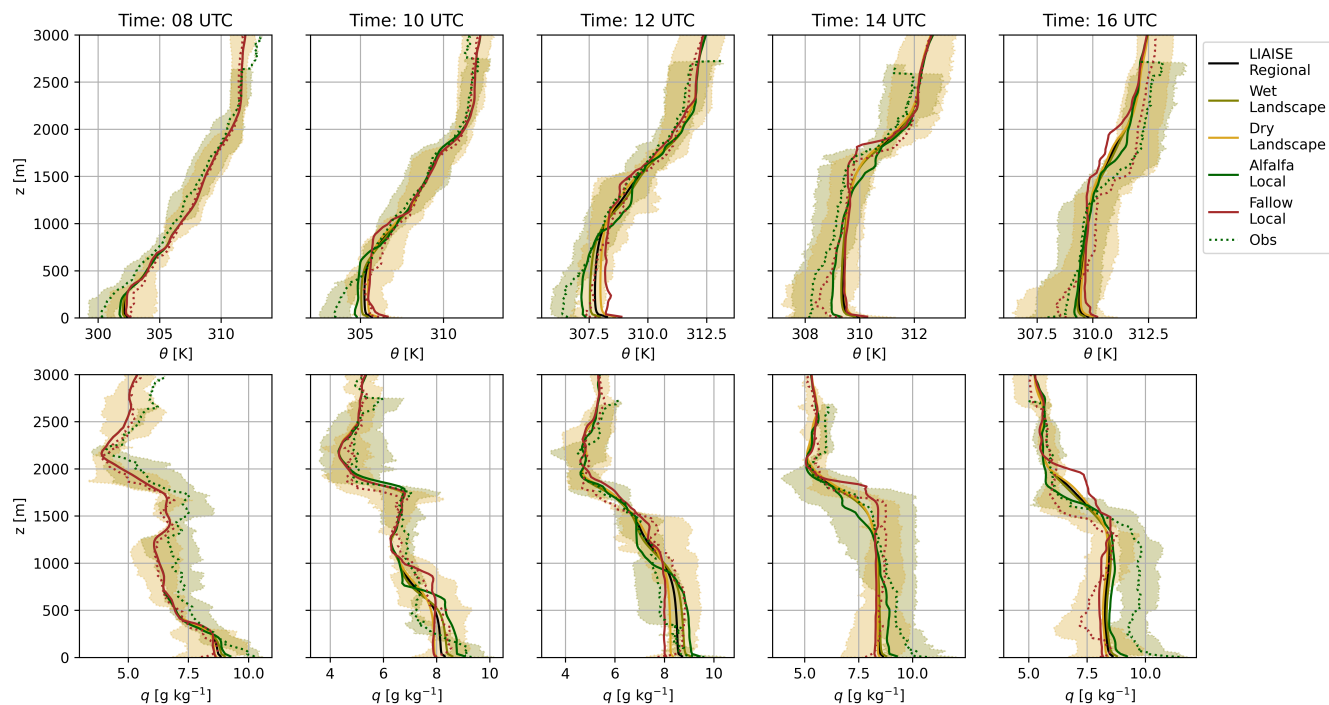


**Figure A1.** The composite LIAISE golden day radiosondes (dotted line and shading) with the spatial averages of the potential temperature and specific humidity from the LES. The colored solid line correspond to the different spatial scales.

0.05), and white indicates the non-blended zones. The black and green lines indicate  $z_i$  of the regional and wet landscape scales respectively.

*Author contributions.* **MRM:** Conceptualization, Methodology, Formal analysis, Writing - original draft & preparation; **JV:** Conceptualization, Supervision, Writing – review & editing; **BvS:** Methodology, Software, Writing – review & editing; **ML:** Data curation, Methodology; **GC:** Data curation, Methodology; **OH:** Conceptualization, Supervision, Writing – review & editing

*Competing interests.* The authors declare that they have no conflict of interest.

**585 Acknowledgements.** We would like to thank the hosts, organizers and participants of the LIAISE campaign. Prof. Kyaw Tha Paw U and Dr. Donald Lenschow provided interesting discussions which influenced sections of this study.

This PhD project partly was supported by the appointment of Jordi Vilà-Guerau de Arellano as Chair of the Meteorology and Air Quality Group of Wageningen University.

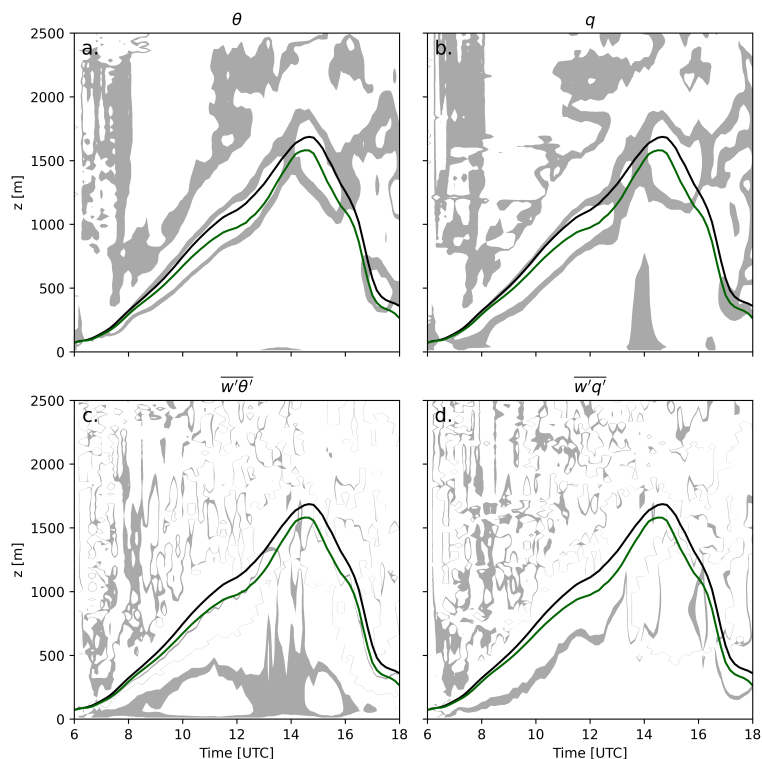


**Figure B1.** Time-height figures for blended variables between the wet landscape and the LIAISE regional scales. The gray colors indicate that the scales are blended at a certain time. The variable are (a) potential temperature, (b) specific humidity, (c) heat flux and (d) moisture flux.

## References

- 590 Aguirre-Correa, F., de Arellano, J. V.-G., Ronda, R., Lobos-Roco, F., Suárez, F., and Hartogensis, O.: Midday Boundary-Layer Collapse in the Altiplano Desert: The Combined Effect of Advection and Subsidence, *Boundary-Layer Meteorol*, <https://doi.org/10.1007/s10546-023-00790-5>, 2023.
- Avissar, R. and Schmidt, T.: An Evaluation of the Scale at which Ground-Surface Heat Flux Patchiness Affects the Convective Boundary Layer Using Large-Eddy Simulations, *Journal of the Atmospheric Sciences*, 55, 2666–2689, [https://doi.org/10.1175/1520-0469\(1998\)055<2666:AEOTSA>2.0.CO;2](https://doi.org/10.1175/1520-0469(1998)055<2666:AEOTSA>2.0.CO;2), 1998.
- 595 Beyrich, F. and Mengelkamp, H.-T.: Evaporation over a Heterogeneous Land Surface: EVA\_GRIPS and the LITFASS-2003 Experiment—An Overview, *Boundary-Layer Meteorol*, 121, 5–32, <https://doi.org/10.1007/s10546-006-9079-z>, 2006.
- Boone, A., Bellvert, J., Best, M., Brooke, J., Canut-Rocafort, G., Cuxart, J., Hartogensis, O., e Moigne, P., Miró, J. R., Polcher, J., Price, J., Quintana Seguí, P., and Wooster, M.: Updates on the International Land Surface Interactions with the Atmosphere over the Iberian
- 600 Semi-Arid Environment (LIAISE) Field Campaign, *GEWEX News*, 31, 17–21, 2021.



- Bou-Zeid, E., Anderson, W., Katul, G. G., and Mahrt, L.: The Persistent Challenge of Surface Heterogeneity in Boundary-Layer Meteorology: A Review, *Boundary-Layer Meteorol*, 177, 227–245, <https://doi.org/10.1007/s10546-020-00551-8>, 2020.
- Brilouet, P.-E., Lothon, M., Etienne, J.-C., Richard, P., Bony, S., Lernoult, J., Bellec, H., Vergez, G., Perrin, T., Delanoë, J., Jiang, T., Pouvesle, F., Lainard, C., Cluzeau, M., Guiraud, L., Medina, P., and Charoy, T.: The EUREC<sup>4</sup>A turbulence dataset derived from the SAFIRE ATR  
605 42 aircraft, *Earth System Science Data*, 13, 3379–3398, <https://doi.org/10.5194/essd-13-3379-2021>, 2021.
- Brunsell, N. A., Mechem, D. B., and Anderson, M. C.: Surface heterogeneity impacts on boundary layer dynamics via energy balance partitioning, *Atmospheric Chemistry and Physics*, 11, 3403–3416, <https://doi.org/10.5194/acp-11-3403-2011>, 2011.
- Butterworth, B. J., Desai, A. R., Townsend, P. A., Petty, G. W., Andresen, C. G., Bertram, T. H., Kruger, E. L., Mineau, J. K., Olson, E. R., Paleri, S., Pertzborn, R. A., Pettersen, C., Stoy, P. C., Thom, J. E., Vermeuel, M. P., Wagner, T. J., Wright, D. B., Zheng, T.,  
610 Metzger, S., Schwartz, M. D., Iglinski, T. J., Mauder, M., Speidel, J., Vogelmann, H., Wanner, L., Augustine, T. J., Brown, W. O. J., Oncley, S. P., Buban, M., Lee, T. R., Cleary, P., Durden, D. J., Florian, C. R., Lantz, K., Riihimaki, L. D., Sedlar, J., Meyers, T. P., Plummer, D. M., Guzman, E. R., Smith, E. N., Sühling, M., Turner, D. D., Wang, Z., White, L. D., and Wilczak, J. M.: Connecting Land–Atmosphere Interactions to Surface Heterogeneity in CHEESEHEAD19, *Bulletin of the American Meteorological Society*, 102, E421–E445, <https://doi.org/10.1175/BAMS-D-19-0346.1>, 2021.
- 615 de Roode, S. R. d., Duynkerke, P. G., and Jonker, H. J. J.: Large-Eddy Simulation: How Large is Large Enough?, *Journal of the Atmospheric Sciences*, 2004.
- Garratt, J. R.: The internal boundary layer — A review, *Boundary-Layer Meteorol*, 50, 171–203, <https://doi.org/10.1007/BF00120524>, 1990.
- Hechtel, L. M., Stull, R. B., and Moeng, C.-H.: The Effects of Nonhomogeneous Surface Fluxes on the Convective Boundary Layer: A Case Study Using Large-Eddy Simulation, *Journal of the Atmospheric Sciences*, 47, 1721–1741, [https://doi.org/10.1175/1520-620469\(1990\)047<1721:TEONSF>2.0.CO;2](https://doi.org/10.1175/1520-620469(1990)047<1721:TEONSF>2.0.CO;2), 1990.
- Hoinka, K. P. and Castro, M. D.: The Iberian Peninsula thermal low, *Quarterly Journal of the Royal Meteorological Society*, 129, 1491–1511, <https://doi.org/10.1256/qj.01.189>, 2003.
- Huang, H.-Y. and Margulis, S. A.: On the impact of surface heterogeneity on a realistic convective boundary layer, *Water Resources Research*, 45, <https://doi.org/10.1029/2008WR007175>, 2009.
- 625 Huang, J., Lee, X., and Patton, E. G.: Dissimilarity of Scalar Transport in the Convective Boundary Layer in Inhomogeneous Landscapes, *Boundary-Layer Meteorol*, 130, 327–345, <https://doi.org/10.1007/s10546-009-9356-8>, 2009.
- Jiménez, M. A., Grau, A., Martínez-Villagrasa, D., and Cuxart, J.: Characterization of the marine-air intrusion Marinada in the eastern Ebro sub-basin, *International Journal of Climatology*, 43, 7682–7699, 2023.
- Jonker, H. J. J., Duynkerke, P. G., and Cuijpers, J. W. M.: Mesoscale Fluctuations in Scalars Generated by Boundary Layer Convection,  
630 1999.
- Kaimal, J. C. and Finnigan, J. J.: *Atmospheric boundary layer flows: their structure and measurement*, Oxford University Press, New York, ISBN 978-0-19-506239-7, 1994.
- Lenschow, D. H. and Stankov, B. B.: Length Scales in the Convective Boundary Layer, *Journal of the Atmospheric Sciences*, 43, 1198–1209, [https://doi.org/10.1175/1520-0469\(1986\)043<1198:LSITCB>2.0.CO;2](https://doi.org/10.1175/1520-0469(1986)043<1198:LSITCB>2.0.CO;2), 1986.
- 635 Liu, G., Sun, J., and Yin, L.: Turbulence Characteristics of the Shear-Free Convective Boundary Layer Driven by Heterogeneous Surface Heating, *Boundary-Layer Meteorol*, 140, 57–71, <https://doi.org/10.1007/s10546-011-9591-7>, 2011.
- Lunel, T., Boone, A. A., and Le Moigne, P.: Irrigation strongly influences near-surface conditions and induces breeze circulation: Observational and model-based evidence, *Quarterly Journal of the Royal Meteorological Society*, <https://doi.org/10.1002/qj.4736>, 2024a.



- Lunel, T., Jimenez, M. A., Cuxart, J., Martinez-Villagrasa, D., Boone, A., and Le Moigne, P.: The *marinada* fall wind in the eastern Ebro sub-basin: physical mechanisms and role of the sea, orography and irrigation, *Atmospheric Chemistry and Physics*, 24, 7637–7666, <https://doi.org/10.5194/acp-24-7637-2024>, publisher: Copernicus GmbH, 2024b.
- Mahrt, L.: Surface Heterogeneity and Vertical Structure of the Boundary Layer, *Boundary-Layer Meteorology*, 96, 33–62, <https://doi.org/10.1023/A:1002482332477>, 2000.
- Mangan, M. R., Oldroyd, H. J., Paw U, K. T., Clay, J. M., Drake, S. A., Kelley, J., and Suvočarev, K.: Integrated Quadrant Analysis: A New Method for Analyzing Turbulent Coherent Structures, *Boundary-Layer Meteorol*, <https://doi.org/10.1007/s10546-022-00694-w>, 2022.
- Mangan, M. R., Hartogensis, O., Boone, A., Branch, O., Canut, G., Cuxart, J., de Boer, H. J., Le Page, M., Martínez-Villagrasa, D., Miró, J. R., Price, J., and Vilà-Guerau de Arellano, J.: The surface-boundary layer connection across spatial scales of irrigation-driven thermal heterogeneity: An integrated data and modeling study of the LIAISE field campaign, *Agricultural and Forest Meteorology*, 335, 109–152, <https://doi.org/10.1016/j.agrformet.2023.109452>, 2023a.
- Mangan, M. R., Hartogensis, O., van Heerwaarden, C., and Vilà-Guerau de Arellano, J.: Evapotranspiration controls across spatial scales of heterogeneity, *Quarterly Journal of the Royal Meteorological Society*, 149, 2696–2718, <https://doi.org/10.1002/qj.4527>, 2023b.
- Maronga, B., Moene, A. F., van Dinter, D., Raasch, S., Bosveld, F. C., and Gioli, B.: Derivation of Structure Parameters of Temperature and Humidity in the Convective Boundary Layer from Large-Eddy Simulations and Implications for the Interpretation of Scintillometer Observations, *Boundary-Layer Meteorol*, 148, 1–30, <https://doi.org/10.1007/s10546-013-9801-6>, 2013.
- Ouwensloot, H. G., Vilà-Guerau de Arellano, J., van Heerwaarden, C. C., Ganzeveld, L. N., Krol, M. C., and Lelieveld, J.: On the segregation of chemical species in a clear boundary layer over heterogeneous land surfaces, *Atmospheric Chemistry and Physics*, 11, 10 681–10 704, <https://doi.org/10.5194/acp-11-10681-2011>, 2011.
- Patton, E. G., Sullivan, P. P., and Moeng, C.-H.: The Influence of Idealized Heterogeneity on Wet and Dry Planetary Boundary Layers Coupled to the Land Surface, *J. Atmos. Sci.*, 62, 2078–2097, <https://doi.org/10.1175/JAS3465.1>, 2005.
- Pino, D., Jonker, H. J. J., Arellano, J. V.-G. d., and Dosio, A.: Role of Shear and the Inversion Strength During Sunset Turbulence Over Land: Characteristic Length Scales, *Boundary-Layer Meteorol*, 121, 537–556, <https://doi.org/10.1007/s10546-006-9080-6>, 2006.
- Raasch, S. and Harbusch, G.: An Analysis Of Secondary Circulations And Their Effects Caused By Small-Scale Surface Inhomogeneities Using Large-Eddy Simulation, *Boundary-Layer Meteorology*, 101, 31–59, <https://doi.org/10.1023/A:1019297504109>, 2001.
- Rappin, E., Mahmood, R., Nair, U., Pielke, R. A., Brown, W., Oncley, S., Wurman, J., Kosiba, K., Kaulfus, A., Phillips, C., Lachenmeier, E., Santanello, J., Kim, E., and Lawston-Parker, P.: The Great Plains Irrigation Experiment (GRAINEX), *Bulletin of the American Meteorological Society*, 102, E1756–E1785, <https://doi.org/10.1175/BAMS-D-20-0041.1>, 2021.
- Shen, S. and Leclerc, M. Y.: How large must surface inhomogeneities be before they influence the convective boundary layer structure? A case study, *Quarterly Journal of the Royal Meteorological Society*, 121, 1209–1228, <https://doi.org/10.1002/qj.49712152603>, 1995.
- Stull, R. B.: *An Introduction of Boundary Layer Meteorology*, Kluwer, Dordrecht, 1988.
- Stull, R. B. and Driedonks, A. G. M.: Applications of the transilient turbulence parameterization to atmospheric boundary-layer simulations, *Boundary-Layer Meteorol*, 40, 209–239, <https://doi.org/10.1007/BF00117449>, 1987.
- van Heerwaarden, C. C. and Vilà Guerau de Arellano, J.: Relative Humidity as an Indicator for Cloud Formation over Heterogeneous Land Surfaces, *Journal of the Atmospheric Sciences*, 65, 3263–3277, <https://doi.org/10.1175/2008JAS2591.1>, 2008.
- van Heerwaarden, C. C., Mellado, J. P., and Lozar, A. D.: Scaling Laws for the Heterogeneously Heated Free Convective Boundary Layer, *Journal of Atmospheric Sciences*, 71, 3975–4000, <https://doi.org/10.1175/JAS-D-13-0383.1>, 2014.



<https://doi.org/10.5194/egusphere-2024-3000>

Preprint. Discussion started: 28 October 2024

© Author(s) 2024. CC BY 4.0 License.



van Heerwaarden, C. C., van Stratum, B. J. H., Heus, T., Gibbs, J. A., Fedorovich, E., and Mellado, J. P.: MicroHH 1.0: a computational fluid dynamics code for direct numerical simulation and large-eddy simulation of atmospheric boundary layer flows, *Geoscientific Model Development*, 10, 3145–3165, <https://doi.org/https://doi.org/10.5194/gmd-10-3145-2017>, 2017.

680 van Stratum, B. J. H., van Heerwaarden, C. C., and Vilà-Guerau de Arellano, J.: The Benefits and Challenges of Downscaling a Global Reanalysis With Doubly-Periodic Large-Eddy Simulations, *Journal of Advances in Modeling Earth Systems*, 15, e2023MS003750, <https://doi.org/10.1029/2023MS003750>, 2023.